



ORIGINAL ARTICLES

Current steering to control the volume of tissue activated during deep brain stimulation

Christopher R. Butson, PhD, Cameron C. McIntyre, PhD

Department of Biomedical Engineering, Cleveland Clinic Foundation, Cleveland, Ohio

Background

Over the last two decades, deep brain stimulation (DBS) has become a recognized and effective clinical therapy for numerous neurologic conditions. Since its inception, clinical DBS technology has progressed at a relatively slow rate; however, numerous advances in neural engineering research have the potential to improve DBS systems. One such advance is the concept of current steering, or the use of multiple stimulation sources to direct current flow through targeted regions of brain tissue. The goals of this study were to develop a theoretical understanding of the effects of current steering in the context of DBS, and use that information to evaluate the potential use of current steering during stimulation of the subthalamic nucleus.

Methods

We used finite element electric field models, coupled to multicompartement cable axon models, to predict the volume of tissue activated (VTA) by DBS as a function of the stimulation parameter settings.

Results

Balancing current flow through adjacent cathodes can increase the VTA magnitude, relative to monopolar stimulation, and current steering can be an effective technique to sculpt the shape of the VTA to fit a given anatomic target.

Conclusions

These results provide motivation for the integration of current steering technology into clinical DBS systems, thereby expanding opportunities to customize DBS to individual patients, and potentially enhancing therapeutic efficacy.

© 2008 Elsevier Inc. All rights reserved.

Keywords electrode; model; electric field; neuromodulation; neurostimulation; subthalamic nucleus

Address reprint requests to: Dr. Cameron C. McIntyre, Department of Biomedical Engineering, Cleveland Clinic Foundation, 9500 Euclid Ave. ND-20, Cleveland, OH 44195.

E-mail address: mcintyc@ccf.org

Submitted July 20, 2007; revised August 28, 2007. Accepted for publication August 28, 2007.

The clinical efficacy of deep brain stimulation (DBS) has been clearly demonstrated for movement disorders,¹⁻³ and DBS also shows promise in the treatment of other neurologic conditions.⁴⁻⁶ Clinical studies have established that the therapeutic outcomes of DBS are strongly dependent on three factors: (1) careful selection of appropriate patients for DBS⁷; (2) accurate surgical placement of the electrode in the target brain region for the given disorder⁸; and (3) attentive patient-specific titration of the stimulation parameter settings.⁹ Electrode placement and stimulation parameter settings synergistically interact to define the therapeutic window for stimulation, or parameter space where stimulation provides therapeutic benefit without stimulation induced side effects. However, once the electrode is implanted, revision surgeries are uncommon, and clinical outcomes are strongly dependent on the ability of the clinician to work within the stimulation capabilities of the implanted pulse generator (IPG).

The majority of DBS patients are presently implanted with IPGs that use single-source, voltage-controlled stimulation. Typically, a single electrode contact is stimulated as a cathode with the IPG case as an anodic return (i.e. monopolar stimulation). If adequate therapeutic effects cannot be achieved with monopolar stimulation, multi-contact stimulation strategies are often attempted. However, because the IPGs rely on a voltage-controlled source, the impedance of the electrode-tissue interface at each active contact will dictate current flow in the tissue. In turn, while these devices allow for simultaneous activation of multiple contacts at a single voltage level, the clinician cannot directly control current flow across the contacts.

An alternative direction for future DBS IPGs is the use of current-controlled stimulation with multiple independent current sources. These features open up opportunities to direct stimulation through multiple electrode contacts with known current delivery to the tissue. This concept, known as current steering, has been used in peripheral nerve cuff electrodes¹⁰ and spinal cord stimulation¹¹ to enable targeted stimulation of specific fiber populations. In turn, it is possible that current steering could find similar use in the context of DBS.

Previously we developed a detailed methodology to predict the volume of tissue activated (VTA) during DBS as a function of electrode design and stimulation parameter settings.^{12,13} This study expands our analysis to consider current steering between two adjacent cathodes on a DBS lead. To provide an example of how current steering could theoretically be used, we considered stimulation of the subthalamic nucleus (STN). STN DBS for the treatment of Parkinson's disease is the most common application of DBS technology, and numerous studies have identified anatomically distinct territories within the subthalamic region that are associated with stimulation efficacy.^{14,15} However, these therapeutic areas are flanked by the internal capsule, a major fiber pathway that when stimulated causes unwanted side effects. In turn, the clinical goal of STN DBS is to maximize stimulation coverage of the therapeutic target area without spreading into side effect areas. The precise anatomical

target volume of tissue that should be stimulated by STN DBS to maximize therapeutic outcome is an area of ongoing research, and outside of the scope of this study. However, to demonstrate the general concept of current steering, we used a 3D model of the STN as a representative stimulation target. Our theoretical results show that current steering can expand opportunities to control the shape of the VTA, and current steering could find clinical use in the sculpting of the VTA to best fit the anatomy of the therapeutic target.

Methods and materials

This study addresses current steering technology in the context of DBS by predicting the activation of axons surrounding the DBS electrode. The underlying therapeutic mechanisms of DBS remain unknown. In turn, it remains unclear what neural response(s) in which anatomic structure(s) are directly responsible for the therapeutic or nontherapeutic effects of the stimulation. Converging computational¹⁶ and experimental¹⁷ results suggest that therapeutic DBS in the STN region generates an excitatory effect on axons surrounding the electrode. Although correlations between axonal activation and the therapeutic mechanisms of DBS remain controversial, one leading hypothesis is that high-frequency stimulation overrides the underlying pathologic neural activity patterns.¹⁸⁻²⁰ Therefore, the approach taken in this study was to address the volume of axonal tissue directly activated by clinically relevant stimulation parameter settings.

The general methodology of this study followed and extended our previous publications.^{13,21-24} Neural stimulation was estimated with an integrated system that combined finite element model (FEM) electric field solutions with multicompartment cable models of myelinated axons. The electric field generated by the DBS electrode was calculated from the Poisson equation with a Fourier FEM solver to determine the time- and space-dependent voltage distribution within the tissue medium.²³ The voltage waveforms were subsequently interpolated onto model axons distributed around the electrode, and threshold values of the stimulation amplitude necessary for action potential generation were calculated. The second spatial difference of the extracellular potential distribution ($\Delta^2 V_e / \Delta x^2$) at the site of action potential initiation in each axon ($\Delta x =$ internodal spacing of 0.5 mm) was calculated at the stimulus threshold for action potential generation. The $\Delta^2 V_e / \Delta x^2$ solutions were then used to create a VTA prediction scheme as a function of stimulation parameters. The VTA prediction scheme was then used in a detailed model of human DBS¹³ to explore how current steering could be used to control the VTA in a clinically relevant context.

Finite element model

An axisymmetric FEM with 17,561 nodes was constructed in COMSOL v3.2 (Comsol Inc, Burlington, Massachusetts) (Figure 1).¹² Electrode dimensions were based on the

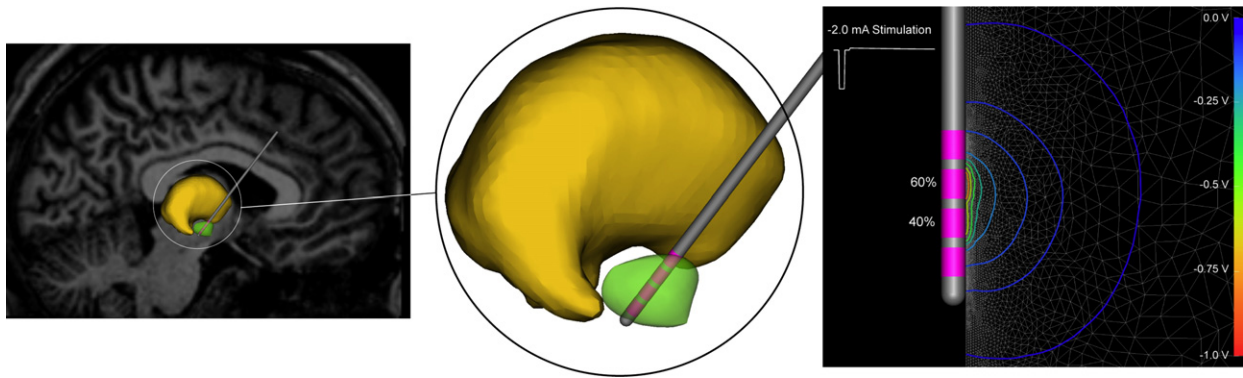


Figure 1 DBS model. The subthalamic nucleus (green volume) represents a common anatomic target for DBS lead (grey shaft, pink electrode contacts) shown passing through the thalamus (yellow volume). The stimulation protocol specified the waveform and the amount of current injected through each contact. The voltage distribution in the tissue medium generated during current-controlled stimulation was determined from a finite element model with the total current amplitude divided between adjacent electrode contacts. DBS, Deep brain stimulation.

Medtronic 3389 quadripolar DBS electrode (contact size = 1.5 mm height, 1.27 mm diameter; contact spacing = 0.5 mm) (Medtronic Inc., Minneapolis, Minnesota). The bulk tissue conductivity was set to 0.2 S/m to mimic neural tissue, and a 0.5 mm thick encapsulation layer with 0.1 S/m conductivity surrounded the electrode.²⁴ The model exhibited an electrode impedance of approximately 1 k Ω , consistent with clinical impedance measurements. In turn, a simple conversion of 1 mA to 1 V can be used to approximate the relative voltage-controlled stimulus magnitudes for the current-controlled stimulation reported in this study. Current was simultaneously injected through two adjacent contacts with specified percentages (0/100, 10/90, 20/80, 30/70, 40/60, 50/50) of the total current diverted to each contact.

The Precision IPG (Advanced Bionics Corp., Valencia, California) represents a commercially available IPG capable of current steering because of its multiple independent current sources. Therefore, we used stimulus waveforms derived from the Precision IPG in our simulations (Figure 1). The waveforms consisted of an initial cathodic phase with a duration specified by the pulse width, a 0.1-msec interpulse delay, and a charge-balancing anodic phase of passive recharge over a 6-msec time window. The current levels specified in the results were equal to the amplitude of the cathodic phase of the waveform. All simulations presented in the results used a 0.1-msec cathodic pulse width and 130 Hz stimulation frequency, consistent with typical clinical DBS parameter settings.

Neural stimulation prediction

Axonal activation was predicted by coupling the DBS FEM to 5.7 μ m diameter myelinated axon models.^{12,25} A collection of 147 model axons were distributed in a 7×21 matrix-oriented perpendicular to the electrode shaft (Figure 2). This orientation of axons was used to identify the spatial extent of activation in the vertical and horizontal directions

relative to the electrode shaft. Each model axon included 21 nodes of Ranvier with 0.5 mm internodal spacing. The time-dependent potential distribution generated in the tissue medium from the DBS FEM solution was interpolated onto the length of each cable model, and the time-dependent transmembrane potentials induced in the axon were calculated in NEURON v5.7.²⁶ Threshold stimulus amplitudes were defined for each axon model such that action potentials were generated in a 1:1 ratio with a stimulus frequency of 130 Hz.

The second difference of the extracellular potential distribution along a neural process ($\Delta^2 V_e / \Delta x^2$) provides an estimate of the polarization of the neuron in response to an applied electric field and can be used to predict action potential initiation.²⁷ However, $\Delta^2 V_e / \Delta x^2$ has limitations as a direct predictor of action potential threshold,²⁸⁻³⁰ and when multiple current sources are active simultaneously, simple relationships between $\Delta^2 V_e / \Delta x^2$ and axonal threshold break down. Therefore, we constructed a prediction scheme for axonal activation based on a weighted sum of the current injected through each active contact divided by the distance from each active contact to each axon. The $\Delta^2 V_e / \Delta x^2$ threshold predictor function was determined by plotting the $\Delta^2 V_e / \Delta x^2$ thresholds versus the normalized electrode-to-axon distance, where normalized distance (D) was defined as:

$$1/D = \left\{ \left[\frac{\text{(contact 1 normalized amplitude)}}{\text{(axon to contact 1 distance)}} \right] + \left[\frac{\text{(contact 2 normalized amplitude)}}{\text{(axon to contact 2 distance)}} \right] \right\}.$$

The resulting data were fit to a curve (Figure 2B), and an analytical predictor was then used to determine $\Delta^2 V_e / \Delta x^2$ thresholds for the given stimulation pulse width (0.1 msec), and frequency (130 Hz):

$$\Delta^2 V_e / \Delta x^2 \text{ threshold} = 12.3 * D^{-0.43}$$

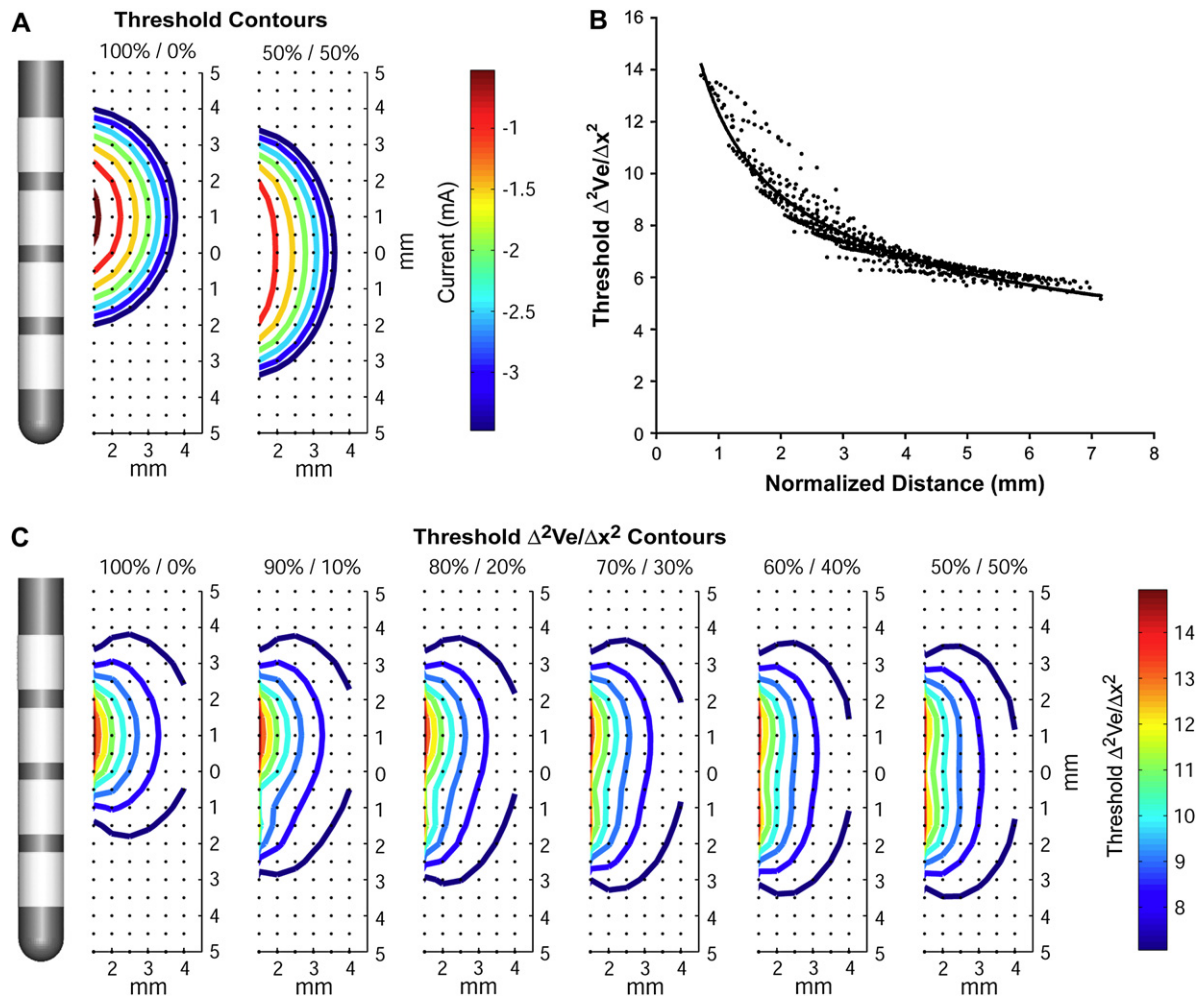


Figure 2 Axonal activation prediction. (A) Axons were distributed in a grid around the DBS electrode (black dots). The voltage within the tissue medium was determined relative to the active DBS contact(s) and the threshold for action potential generation in each axon was defined. (B, C) The second spatial difference of the extracellular voltage at threshold was calculated for each axon as a function of distance from the electrode for a range of current amplitudes and percentage mixtures between adjacent contacts. A predictor curve was generated by aggregating the data and fitting it to an exponential function. DBS, Deep brain stimulation.

Human DBS model

The Butson et al.¹³ human DBS model was designed to provide anatomically and electrically accurate predictions of the VTA as a function of the stimulation parameter settings. The model included the capacitance of the electrode-tissue interface and electrode encapsulation described above, as well as explicit representation of the 3-dimensional (3D) anisotropic and inhomogeneous tissue electrical properties that surround STN DBS electrodes. We converted the Wakana et al.³¹ diffusion tensor MRI atlas brain into a set of conductivity tensors as described by Tuch et al.³² These conductivity tensors were then mapped into a 3D finite element mesh, allowing for solution of the time- and space-dependent potential distribution generated by a DBS electrode implanted in the STN.¹³ The model system also included 3D anatomic volumes of individual brain nuclei warped to the MRI, thereby allowing estimates of the anatomic borders of the STN.

The human DBS model simulations were performed on an 8 processor SGI Prism (Silicon Graphics Inc, Mountain View, California) with 36 GB of shared memory using SCIRun/BioPSE (Scientific Computing & Imaging Institute, University of Utah, Salt Lake City, Utah). The FEM solution created a potential distribution (V_e) in the tissue medium that was dependent on the electrode location in the brain and the stimulation parameter settings. In turn, we calculated the $\Delta^2 V_e / \Delta x^2$, and used the current steering $\Delta^2 V_e / \Delta x^2$ threshold predictor function (Figure 2) to define 3D surfaces that encompassed the volume of tissue supra-threshold for axonal activation for the given stimulation parameter settings (Figures 4 and 5).

Results

Monopolar DBS with either current-controlled stimulation (Precision IPG—as performed in this study) or

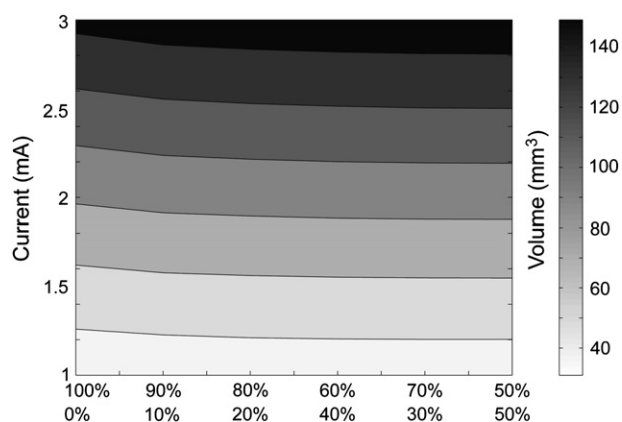


Figure 3 Current steering VTA. Contour plot of the volume of tissue activated as a function of stimulus amplitude and the percentage of current delivered through each electrode contact. VTA, Volume of tissue activated.

voltage-controlled stimulation (Soletra IPG—as performed in Butson et al.)¹² generated nearly identical VTA shapes. However, when incremental amounts of current were diverted to an adjacent electrode contact, the shape of the VTA changed (Figure 2). The pseudo-sphere shape of the monopolar VTA morphed to a pear shape under conditions of 90/10, 80/20, 70/30, and under conditions of 60/40, 50/50, the VTA became more cylindrical. Balancing the current across 2 contacts also increased the total activated volume, relative to monopolar stimulation, with the greatest increase at 50/50 (eg, 90/10 generated a 3% increase; 70/30 a 5% increase; 50/50 a 6% increase) (Figure 3).

Simulations performed in the human model of STN DBS showed that the physical relationship between the VTA and the STN anatomy could be controlled with greater specificity by using current steering than with monopolar stimulation alone (Figure 4). Transitioning from contact 1 to contact 2, the use of current steering allowed for incremental activation of the tissue region between contacts and expanded opportunities to sculpt the VTA to fit the anatomic target. For example, monopolar stimulation at contact 2 activated 21 mm³ of the STN at -0.7 mA before the VTA spread outside the borders of the STN. Similarly, monopolar stimulation of -1.6 mA could be delivered through contact 1 to activate 45 mm³. However, current steering with an injection of -0.36 mA at contact 1 and -1.44 mA at contact 2 (20/80 split of -1.8 mA) activated 63 mm³ of the STN without spreading into neighboring structures (Figure 5).

Discussion

The goals of this study were as follows: (1) to develop quantitative techniques for predicting the DBS VTA when balancing specific amounts of current through adjacent electrode contacts, and (2) to theoretically evaluate the clinical utility of using current steering to control the VTA.

The results show that balancing current delivery across two contacts increases the size of the VTA, compared with monopolar stimulation. Further, current steering can be used to sculpt the VTA to achieve the desired overlap with target tissue structures. This additional functionality may expand opportunities to achieve therapeutically optimal stimulation in a given patient. The important engineering designation that enables “steering” is the concept of independent sources (voltage or current). It would also be possible to manipulate the shape of the VTA with voltage steering, given that independent voltage sources were available on the IPG. However, current-controlled stimulation provides assurance that the current delivered to the tissue is consistent and unaffected by changes in the impedance of the electrode-tissue interface.

Clinical DBS parameter selection is an art that balances stimulation induced therapeutic benefit while trying to avoid any stimulation induced side effects.⁹ This process can be difficult and time consuming, and the outcomes are strongly dependent on the experience of the programming clinician.^{33,34} The results of this study show that it is theoretically possible to sculpt the VTA with current steering to maximize stimulation coverage of a given anatomic target (ie, the STN). However, clinical identification of the theoretically optimal stimulation parameter setting may not be intuitively obvious without computational assistance. And, many of the symptoms of neurologic disorders treated with DBS do not provide instantaneous clinical feedback on their control (or lack thereof) as stimulation parameter settings are changed. To address these issues, multiple groups have been working to develop 3D visualization systems that use engineering optimization to predict theoretically optimal electrode placements and stimulation parameter settings.³⁵⁻³⁸ However, the prospect of using patient-specific computer models to augment clinical DBS practices requires two important pieces of *a priori* information: (1) precise knowledge of the DBS electrode location in the anatomy, and (2) clear definition of the therapeutic target volume of tissue that should be stimulated. Unfortunately, given existing imaging techniques and scientific understanding, substantial limitations surround both of these prerequisites.

Identifying the location of DBS electrodes in postoperative MRIs is complicated by the metallic artifact generated by the contacts, and although postoperative computed tomograms (CTs) can provide a more accurate estimate of the 3D electrode location relative to the skull, the image must be coregistered with an MRI to provide neuroanatomic detail. Because of artifact and/or registration errors, current imaging technology can only provide an estimate to within approximately 1 mm of the true location of the electrode in the brain anatomy.^{13,14} Uncertainties of this magnitude have not substantially impacted clinical care in the past because postoperative imaging data are not extensively used to guide the stimulation parameter selection process under existing practices. However, as DBS electrodes

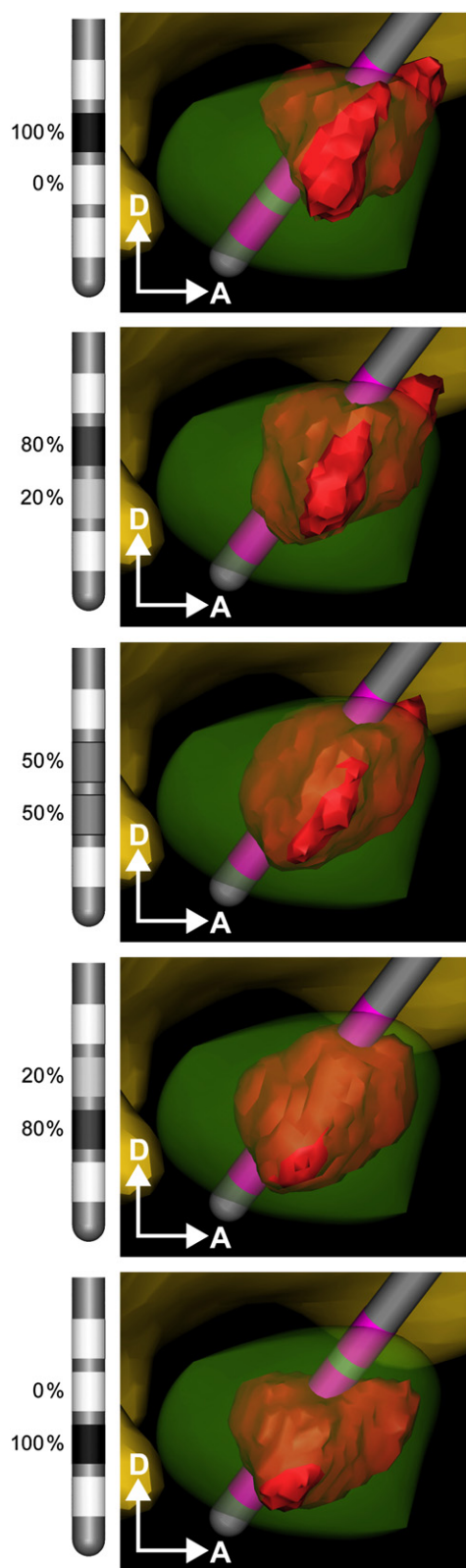


Figure 4 Current steering in the STN. A diffusion-tensor-based 3D FEM of DBS was used to predict the VTA (red volume) from various percentage mixtures of current delivery through 2 DBS contacts in the STN. The stimulation parameters were held constant with 0.1 msec pulses delivered at 130 Hz and at a total

and IPGs become more advanced, detailed knowledge of the lead location in the anatomy will be especially important in defining the electrode contacts and stimulation paradigms that maximize device use in specific patients.

To provide a clinically relevant example of how current steering might be used in DBS, we examined stimulation of the STN. Extensive effort has been dedicated to identifying the anatomic location of therapeutic electrode contacts in the STN region.^{14,15,39-49} The results of these studies suggest that stimulation of the STN per se may not be the only anatomic structure in the region responsible for therapeutic benefit. However, aside from detailed modeling studies of 2 patients,^{13,50} estimates of the electrical spread of stimulation, and its overlap with various anatomic entities in the STN region, have not been correlated with therapeutic outcomes. In turn, scientific definition of the target volume of tissue that should be stimulated for maximal therapeutic benefit remains an issue of debate.

For simplicity we used the atlas-defined anatomic borders of the STN to represent our target volume of stimulation, and we placed the DBS electrode in the center of the STN. However, the numerous anatomic studies of DBS electrode implant locations have shown substantial variability across patients. This variability in electrode placement can be attributed to multiple factors (stereotactic frame accuracy, surgical philosophy on target coordinates, and/or use of microelectrode recordings), but the end result is that not every electrode will be perfectly placed in the intended target region. In turn, techniques like current steering, that expand the stimulation coverage and/or flexibility of any given implanted electrode, could be an important asset in a clinical setting. However, when defining therapeutic stimulation parameter settings in a patient, it is unrealistic to clinically evaluate each of the thousands of different stimulation parameter settings available for a given electrode and IPG model. Therefore, new clinical stimulation parameter selection techniques will be necessary to maximize the use of advanced DBS systems. Assuming that the above-mentioned limitations in imaging and stimulation target definition can be resolved, coupling current steering DBS technology with computer-assisted patient-specific stimulation parameter selection may be an attractive option for the future.

Predicting the spread of stimulation during DBS requires the definition of a neural response outcome measure. The VTA predictions used in this study represent simplified estimates of the response of myelinated axons to DBS. We originally developed the general threshold prediction scheme used in this study to address monopolar

current of 2 mA. VTAs are shown as a function of different current mixtures from 100%/0% (monopolar on contact 2) to 50%/50% (through contacts 1 and 2) to 0%/100% (monopolar on contact 1). STN, Subthalamic nucleus; 3D, 3 dimensional; FEM, finite element model; DBS, deep brain stimulation; VTA, volume of tissue activated.

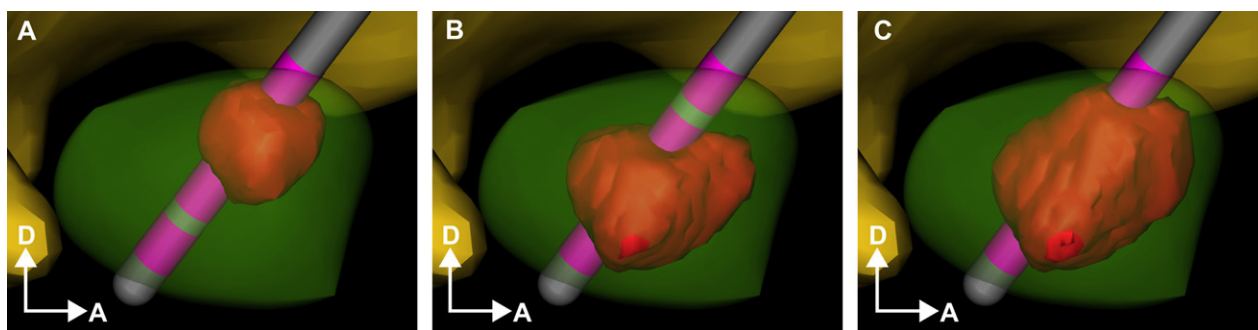


Figure 5 STN constrained stimulation. (A) Monopolar stimulation through contact 2 was increased from 0 to -0.7 mA before the VTA spread beyond the borders of the STN. Note that the VTA first spreads beyond the STN on the medial side (not visible from this view). (B) Monopolar stimulation through contact 1 could be increased to -1.6 mA before spreading beyond the borders of the STN. (C) Controlled mixing of -1.8 mA through contact 1 (80%) and contact 2 (20%) stimulated 63 mm^3 of the STN without spreading into neighboring structures. STN, Subthalamic nucleus; VTA, volume of tissue activated.

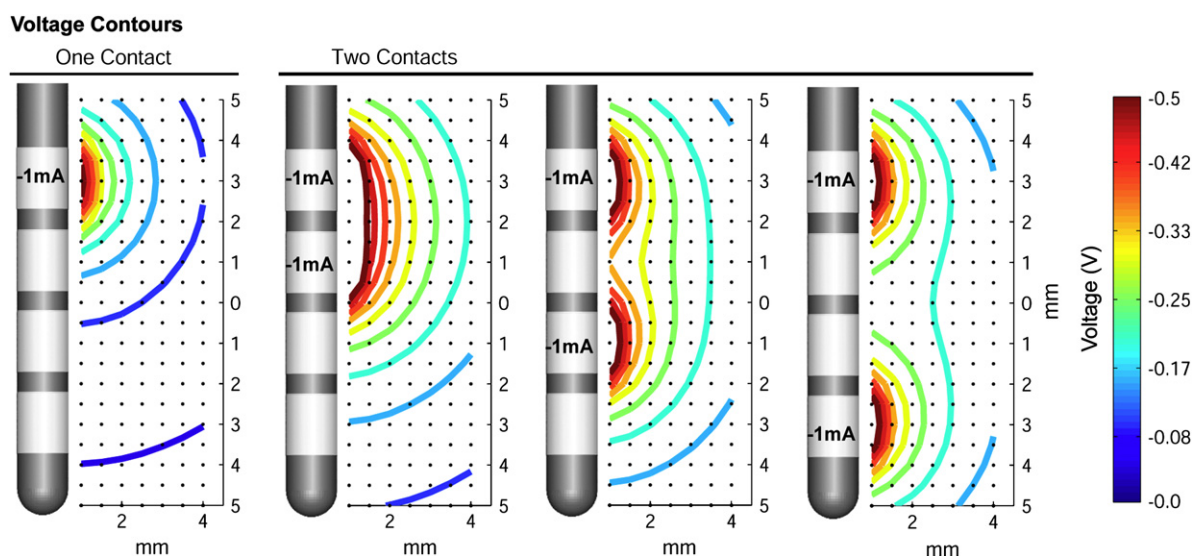


Figure 6 Effects of electrode contact spacing on voltage distribution. The effects of contact spacing are shown by comparing current injection through one contact (leftmost panel) to injection through two contacts. The current injected is indicated on each electrode contact, and the resulting distribution is represented by isovoltage contours according to the color bar at right. The voltage distributions from adjacent active contacts show substantial overlap (2nd panel from left), while the presence of one or more intervening dormant contacts results in separate distributions that approach the single contact configuration (rightmost two panels).

stimulation.¹² We have attempted to validate this technique by comparing our model predictions of axonal activation to clinical measurements of internal capsule activation (ie, DBS induced EMG thresholds from corticospinal tract activation).¹³ When adapting this methodology to study current steering it became readily apparent that both active electrode contacts needed to be considered in the prediction scheme. Several formulas were evaluated, and the solution presented in the Methods provided the best overall fit to our data. However, alternative techniques may provide more accurate solutions in the future.

Our previous theoretical and experimental analysis suggests that interesting correlations can be defined between axonal activation and therapeutic DBS.^{13,16} However, several important underlying assumptions in our

study should be noted. First, the tissue medium was undifferentiated with regard to the distribution of myelinated axons. Second, activation of more tissue was considered better than less. Third, there was no relative benefit to stimulation of different sub-regions of tissue in the target volume. In addition, it is distinctly possible that the underlying therapeutic effects of DBS are actually related to neural responses unconnected to axonal activation. Nonetheless, the basic mechanisms of DBS are related to modulating neural activity with electric fields, and current steering represents an additional tool to enhance control of the applied electric field.

Three general design techniques exist to control the electric field generated by DBS: (1) construction of the stimulus waveform/train,⁵¹⁻⁵³ (2) shape of the electrode contact,^{12,54,55} and (3) configuration of active electrode

contacts.^{21,56} This study focused on one aspect of the configuration of active electrode contacts (ie, current steering between adjacent cathodes). However, numerous questions remain to be addressed on all of the above mentioned DBS design techniques. For example, in relation to current steering a logical next step is evaluation of the spacing between contacts. Figure 6 shows the voltage distribution generated by simultaneous activation of two DBS contacts with various spacing. These different voltage distributions will result in different VTA shapes and thereby provide additional opportunities to customize the shape of the VTA.

In summary, the results of this study show that current steering can expand opportunities to sculpt DBS to fit the anatomic target of the stimulation. However, numerous technical hurdles remain before the full spectrum of DBS technology can be optimally used in clinical settings. In turn, future improvements in DBS systems will rely on parallel development of engineering hardware (for example, advanced stereotactic targeting, IPG technology), computer software (namely, 3D visualization, optimization algorithms), imaging technology (for example, advanced imaging sequences, intraoperative imaging), and clinical training on maximizing the use of these new technologies.

Acknowledgment

This work was supported by funding from the National Institutes of Health (NS050449, NS052042, NS059736) and Advanced Bionics Corporation. The authors also thank Susumu Mori for providing the diffusion tensor brain atlas data set and Jaimie Henderson for providing the 3D brain atlas volumes.

CRB and CCM are paid consultants for the Advanced Bionics Corporation (a company that owns intellectual property related to current steering), and shareholders in IntElect Medical Inc. (a company that owns intellectual property related to the modeling methodology used in this study).

References

1. Obeso JA, Olanow CW, Rodriguez-Oroz MC, et al. Deep-brain stimulation of the subthalamic nucleus or the pars interna of the globus pallidus in Parkinson's disease. *N Engl J Med* 2001;345:956-963.
2. Benabid AL, Pollak P, Gao D, et al. Chronic electrical stimulation of the ventralis intermedius nucleus of the thalamus as a treatment of movement disorders. *J Neurosurg* 1996;84:203-214.
3. Vidailhet M, Vercueil L, Houeto JL, et al. Bilateral deep-brain stimulation of the globus pallidus in primary generalized dystonia. *N Engl J Med* 2005;352:459-467.
4. Hodaie M, Wennberg RA, Dostrovsky JO, Lozano AM. Chronic anterior thalamus stimulation for intractable epilepsy. *Epilepsia* 2002;43:603-608.
5. Mayberg HS, Lozano AM, Voon V, et al. Deep brain stimulation for treatment-resistant depression. *Neuron* 2005;45:651-660.
6. Nuttin BJ, Gabriels LA, Cosyns PR, et al. Long-term electrical capsular stimulation in patients with obsessive-compulsive disorder. *Neurosurgery* 2003;52:1263-1272; discussion 72-74.
7. Walter BL, Vitek JL. Surgical treatment for Parkinson's disease. *Lancet Neurol* 2004;3:719-728.
8. Machado A, Rezaei AR, Kopell BH, et al. Deep brain stimulation for Parkinson's disease: surgical technique and perioperative management. *Mov Disord* 2006;21(Suppl 14):S247-S258.
9. Volkmann J, Moro E, Pahwa R. Basic algorithms for the programming of deep brain stimulation in Parkinson's disease. *Mov Disord* 2006;21(S14):S284-S289.
10. Veraart C, Grill WM, Mortimer JT. Selective control of muscle activation with a multipolar nerve cuff electrode. *IEEE Trans Biomed Eng* 1993;40:640-653.
11. Alo KM, Holsheimer J. New trends in neuromodulation for the management of neuropathic pain. *Neurosurgery* 2002;50:690-703; discussion 703-704.
12. Butson CR, McIntyre CC. Role of electrode design on the volume of tissue activated during deep brain stimulation. *J Neural Eng* 2006;3:1-8.
13. Butson CR, Cooper SE, Henderson JM, McIntyre CC. Patient-specific analysis of the volume of tissue activated during deep brain stimulation. *NeuroImage* 2007;34:661-670.
14. Yelnik J, Damier P, Demeret S, et al. Localization of stimulating electrodes in patients with Parkinson disease by using a three-dimensional atlas-magnetic resonance imaging coregistration method. *J Neurosurg* 2003;99:89-99.
15. Plaha P, Ben-Shlomo Y, Patel NK, Gill SS. Stimulation of the caudal zona incerta is superior to stimulation of the subthalamic nucleus in improving contralateral parkinsonism. *Brain* 2006;129(Pt 7):1732-1747.
16. Miocinovic S, Parent M, Butson CR, et al. Computational analysis of subthalamic nucleus and lenticular fasciculus activation during therapeutic deep brain stimulation. *J Neurophysiol* 2006;96:1569-1580.
17. Hashimoto T, Elder CM, Okun MS, Patrick SK, Vitek JL. Stimulation of the subthalamic nucleus changes the firing pattern of pallidal neurons. *J Neurosci* 2003;23:1916-1923.
18. Montgomery EB Jr, Baker KB. Mechanisms of deep brain stimulation and future technical developments. *Neurol Res* 2000;22:259-266.
19. Grill WM, Snyder AN, Miocinovic S. Deep brain stimulation creates an informational lesion of the stimulated nucleus. *Neuroreport* 2004;15:1137-1140.
20. Rubin JE, Terman D. High frequency stimulation of the subthalamic nucleus eliminates pathological thalamic rhythmicity in a computational model. *J Comput Neurosci* 2004;16:211-235.
21. McIntyre CC, Mori S, Sherman DL, Thakor NV, Vitek JL. Electric field and stimulating influence generated by deep brain stimulation of the subthalamic nucleus. *Clin Neurophysiol* 2004;115:589-595.
22. McIntyre CC, Savasta M, Walter BL, Vitek JL. How does deep brain stimulation work? Present understanding and future questions. *J Clin Neurophysiol* 2004;21:40-50.
23. Butson CR, McIntyre CC. Tissue and electrode capacitance reduce neural activation volumes during deep brain stimulation. *Clin Neurophysiol* 2005;116:2490-2500.
24. Butson CR, Moks CB, McIntyre CC. Sources and effects of electrode impedance during deep brain stimulation. *Clin Neurophysiol* 2006;117:447-454.
25. McIntyre CC, Richardson AG, Grill WM. Modeling the excitability of mammalian nerve fibers: influence of afterpotentials on the recovery cycle. *J Neurophysiol* 2002;87:995-1006.
26. Hines ML, Carnevale NT. The NEURON simulation environment. *Neural Comput* 1997;9:1179-1209.
27. Rattay F. Analysis of models for external stimulation of axons. *IEEE Trans Biomed Eng* 1986;33:974-977.
28. Moffitt MA, McIntyre CC, Grill WM. Prediction of myelinated nerve fiber stimulation thresholds: limitations of linear models. *IEEE Trans Biomed Eng* 2004;51:229-236.

29. Zierhofer CM. Analysis of a linear model for electrical stimulation of axons-critical remarks on the “activating function concept.” *IEEE Trans Biomed Eng* 2001;48:173-184.
30. Warman EN, Grill WM, Durand D. Modeling the effects of electric fields on nerve fibers: determination of excitation thresholds. *IEEE Trans Biomed Eng* 1992;39:1244-1254.
31. Wakana S, Jiang H, Nagae-Poetscher LM, van Zijl PC, Mori S. Fiber tract-based atlas of human white matter anatomy. *Radiology* 2004; 230:77-87.
32. Tuch DS, Wedeen VJ, Dale AM, George JS, Belliveau JW. Conductivity tensor mapping of the human brain using diffusion tensor MRI. *Proc Natl Acad Sci U S A* 2001;98:11697-11701.
33. Moro E, Poon YY, Lozano AM, Saint-Cyr JA, Lang AE. Subthalamic nucleus stimulation: improvements in outcome with reprogramming. *Arch Neurol* 2006;63:1266-1272.
34. Hunka K, Suchowersky O, Wood S, Derwent L, Kiss ZH. Nursing time to program and assess deep brain stimulators in movement disorder patients. *J Neurosci Nurs* 2005;37:204-210.
35. Butson CR, Noecker AM, Maks CB, McIntyre CC. StimExplorer: deep brain stimulation parameter selection software system. *Acta Neurochir Suppl (Wien)* 2007;97:569-574.
36. D’Haese PF, Cetinkaya E, Konrad PE, Kao C, Dawant BM. Computer-aided placement of deep brain stimulators: from planning to intraoperative guidance. *IEEE Trans Med Imaging* 2005;24:1469-1478.
37. Finnis KW, Starreveld YP, Parrent AG, Sadikot AF, Peters TM. Three-dimensional database of subcortical electrophysiology for image-guided stereotactic functional neurosurgery. *IEEE Trans Med Imaging* 2003;22:93-104.
38. Miocinovic S, Maks CB, Noecker AM, Butson CR, McIntyre CC. Cicero: deep brain stimulation neurosurgical navigation software system. *Acta Neurochir Suppl (Wien)* 2007;97:561-567.
39. Starr PA, Christine CW, Theodosopoulos PV, et al. Implantation of deep brain stimulators into the subthalamic nucleus: technical approach and magnetic resonance imaging-verified lead locations. *J Neurosurg* 2002;97:370-387.
40. Saint-Cyr JA, Hoque T, Pereira LC, et al. Localization of clinically effective stimulating electrodes in the human subthalamic nucleus on magnetic resonance imaging. *J Neurosurg* 2002;97:1152-1166.
41. Lanotte MM, Rizzone M, Bergamasco B, et al. Deep brain stimulation of the subthalamic nucleus: anatomical, neurophysiological, and outcome correlations with the effects of stimulation. *J Neurol Neurosurg Psychiatry* 2002;72:53-58.
42. Hamel W, Fietzek U, Morsnowski A, et al. Deep brain stimulation of the subthalamic nucleus in Parkinson’s disease: evaluation of active electrode contacts. *J Neurol Neurosurg Psychiatry* 2003;74:1036-1046.
43. Voges J, Volkmann J, Allert N, et al. Bilateral high-frequency stimulation in the subthalamic nucleus for the treatment of Parkinson disease: correlation of therapeutic effect with anatomical electrode position. *J Neurosurg* 2002;96:269-279.
44. Zonenshayn M, Sterio D, Kelly PJ, Rezai AR, Beric A. Location of the active contact within the subthalamic nucleus (STN) in the treatment of idiopathic Parkinson’s disease. *Surg Neurol* 2004;62: 216-225.
45. Herzog J, Fietzek U, Hamel W, et al. Most effective stimulation site in subthalamic deep brain stimulation for Parkinson’s disease. *Mov Disord* 2004;19:1050-1054.
46. Nowinski WL, Belov D, Pollak P, Benabid AL. Statistical analysis of 168 bilateral subthalamic nucleus implantations by means of the probabilistic functional atlas. *Neurosurgery* 2005;57(4 Suppl): 319-330.
47. Guehl D, Edwards R, Cuny E, et al. Statistical determination of the optimal subthalamic nucleus stimulation site in patients with Parkinson disease. *J Neurosurg* 2007;106:101-110.
48. Yokoyama T, Ando N, Sugiyama K, Akamine S, Namba H. Relationship of stimulation site location within the subthalamic nucleus region to clinical effects on parkinsonian symptoms. *Stereotact Funct Neurosurg* 2006;84:170-175.
49. Godinho F, Thobois S, Magnin M, et al. Subthalamic nucleus stimulation in Parkinson’s disease: anatomical and electrophysiological localization of active contacts. *J Neurol* 2006;253:1347-1355.
50. Butson CR, Cooper SE, Henderson JM, McIntyre CC. Predicting the effects of deep brain stimulation with diffusion tensor based electric field models. *Med Image Comput Comput Assist Interv* 2006; 9(Pt 2):429-437.
51. McIntyre CC, Grill WM. Extracellular stimulation of central neurons: influence of stimulus waveform and frequency on neuronal output. *J Neurophysiol* 2002;88:1592-1604.
52. Jezernik S, Morari M. Energy-optimal electrical excitation of nerve fibers. *IEEE Trans Biomed Eng* 2005 Apr;52(4):740-743.
53. Sahin M, Tie Y. Non-rectangular waveforms for neural stimulation with practical electrodes. *J Neural Eng* 2007;4:227-233.
54. Wei XF, Grill WM. Current density distributions, field distributions and impedance analysis of segmented deep brain stimulation electrodes. *J Neural Eng* 2005 Dec;2(4):139-147.
55. Gimsa U, Schreiber U, Habel B, Flehr J, van Rienen U, Gimsa J. Matching geometry and stimulation parameters of electrodes for deep brain stimulation experiments—numerical considerations. *J Neurosci Methods* 2006 Jan 30;150(2):212-227.
56. Kuncel AM, Grill WM. Selection of stimulus parameters for deep brain stimulation. *Clin Neurophysiol* 2004 Nov;115(11):2431-2441.